Nano Research

Open Access

Research Article

Theoretical studies of nitrogen-doped graphene loaded transition metal single-atom catalysts for electrochemical CO reduction

Yongze Gao[1], Shamraiz Hussain Talib[2], and Qi Yu[1]✉

[1] School of Materials Science and Engineering, and Shaanxi Laboratory of Catalysis, Shaanxi University of Technology, Hanzhong 723001, China
[2] Center for Catalysis and Separations, Khalifa University of Science and Technology, Abu Dhabi, P.O. Box 127788, United Arab Emirates

Cite this article: *Nano Research*, **2025**, *18*, 94907026. https://doi.org/10.26599/NR.2025.94907026

ABSTRACT: The electrochemical carbon monoxide reduction reaction (CORR) holds significant potential for sustainable fuel and chemical production, offering an effective means to reduce carbon emissions and maintain environmental sustainability. Graphene, a single layer of carbon atoms arranged in a unique two-dimensional structure, possesses properties that make it suitable for various applications. Nitrogen-doped graphene (NDG) based metal single-atom catalysts (SACs) have emerged as one of the most effective methods for converting CO into one carbon (C_1) products such as CH_4 and CH_3OH. In this study, defective graphene was doped with four nitrogen atoms, which stabilized the catalyst through complexation with metal species by binding with the nitrogen atoms. First-principles calculations were employed to investigate the catalytic performance of selected transition metals (TM_1 = Sc, Ti, V, Cr, Mn, Fe, Co, Ni and Cu) as SACs anchored on the NDG surface for hydrogen evolution reaction (HER) and CORR processes. Theoretical analysis indicated that NDG is highly favorable for binding transition metal single adatoms with excellent stability, facilitating rapid electron transfer during catalysis and yielding outstanding catalytic performance. Among the SACs, Cr supported by N_4-G catalyst selectively produces CH_4 with Cr-N_4-G exhibiting the lowest overpotential of 0.47 eV. This study demonstrates that the N_4-G support is a promising candidate for use as a single-atom catalyst for selective CO reduction and other electrochemical processes.

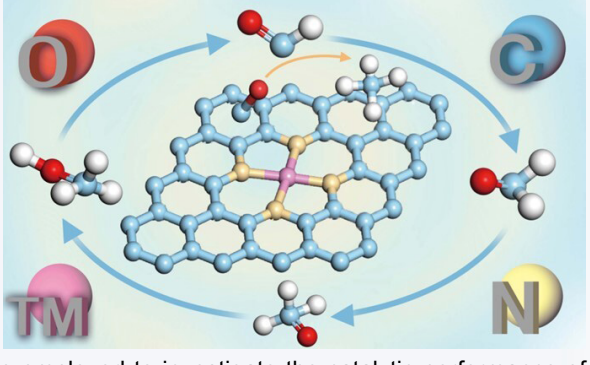

KEYWORDS: CO reduction, nitrogen-doped graphene, single-atom catalysts, density functional theory

1 Introduction

Over the past few decades, scientists and technologists have diligently worked to mitigate carbon monoxide (CO) and carbon dioxide (CO_2) emissions. However, the emissions of these gases remain inevitable due to the advancement of science and technology. Consequently, reducing CO emissions has become an urgent priority for modern society and the development of a sustainable global community. By leveraging green and renewable energy sources, CO can be electrochemically converted into valuable, green and environmentally friendly hydrocarbons. The electrochemical carbon monoxide reduction reaction (CORR), which transforms CO into green and organic hydrocarbons using renewable electricity, plays a crucial role in restoring the carbon balance and closing the carbon cycle [1–3]. Despite the unique advantages, such as compatibility with renewable energy sources and industrial applications, the inert chemical nature of CO limits the activity and selectivity of CORR. To address this challenge, several catalysts, including transition metal (TM) single-atom (SA) catalysts (SACs) [4, 5], have been developed to enhance CORR activity and selectivity [6–15].

Graphene has been extensively studied due to its unique structural features and numerous outstanding properties [16]. These properties include a large surface area, high carrier mobility and exceptional electrical and thermal conductivity [17, 18]. Li et al. [19] focused on the stability of metal SAs on different sites of graphene and their catalytic performance in various chemical reactions, including thermocatalysis and electrocatalysis. They found that graphene-based SACs have simple yet efficient catalytic active centers. Building on this, Chen et al. [20] studied Zn-N-G catalysts for electrocatalytic CO_2 reduction. The addition of Zn-N_x active sites lowered the energy barrier for COOH* and CO*

Received: July 29, 2024; **Revised:** August 28, 2024
Accepted: September 5, 2024

✉Address correspondence to qiyu@snut.edu.cn

intermediates, making it easier to produce CO and other one carbon (C_1) products. This also demonstrated the stability and excellent catalytic properties of graphene as a substrate, particularly for CO_2/CO reduction reactions. As a result, graphene serves as an excellent substrate for the electrochemical CORR. One flexible approach is to use TM frameworks in combination with graphene, which helps overcome the low CO reduction efficiency associated with the neutral carbon atoms in graphene. TM SACs on graphene exhibit unique advantages in terms of activity and selectivity for CORR [21, 22]. Additionally, numerous theoretical and experimental studies have demonstrated the effectiveness of doping graphene with heteroatoms such as boron, nitrogen and phosphorus. These modifications, particularly with nitrogen atoms, can significantly enhance the catalytic performance for CO reduction reactions [23, 24]. Nitrogen doping promotes the formation of H-terminated edges of sp2 carbon, leading to the creation of graphene fibers made of vertically stacked graphene flakes [25]. Additionally, N is commonly used in doped graphene due to its higher electronegativity (N 3.04, C 2.55) and similar atomic size to C. The increased electronegativity of N causes charge redistribution between N and neighboring C atoms, resulting in a positive charge and high spin density, which enhances CORR catalytic activity [26]. Therefore, the mechanism of CO reduction by electrocatalysis using nitrogen-doped graphene (NDG) loaded with TM SACs is of great application value. In general, there are four forms of NDG, which are TM-N_1-G, TM-N_2-G, TM-N_3-G, TM-N_4-G (Fig. S1 in the Electronic Supplementary Material (ESM)).

In this study, we comprehensively investigate single TM atom (STMA = Sc, Ti, V, Cr, Mn, Fe, Co, Ni and Cu) catalysts anchored on NDG (TM-N_4-G) by using density functional theory (DFT), focusing on the electronic structure, geometric stability, catalytic activity and CO adsorption characteristics of TM-N_4-G. On this basis, we systematically explore the electrochemical catalytic mechanisms of CORR on these catalysts. By calculating the adsorption energy and examining the competition between CORR and the hydrogen evolution reaction (HER), meanwhile, Ni-N_4-G and Cu-N_4-G are excluded due to the weak CO adsorption and the TM-N_4-G catalysts are analyzed for free energy calculations. Computational results reveal that C_1 compounds can be synthesized using TM species with low overpotentials (η). Specifically, Cr-N_4-G SACs demonstrate an overpotential of 0.47 eV for the production of H_2O, making it a relatively effective SAC among the investigated NDG loaded TM catalysts for CORR. Based on these findings, the projected TM-N_4-G SACs are promising electrochemical catalytic platforms for the selective conversion of CO into valuable compounds.

2 Computational details

DFT method implemented in Device Studio (DS) [27] was used for all spin-polarized calculations. To describe electron–ion interactions, scalar relativistic effect projector-augmented waves (PAW) [27, 28] methods were used in conjunction with generalized gradient approximation (GGA) and Perdew–Burke–Ernzerh (PBE) [29] functionals to handle electron exchange and related energy. For the planewave basis set, a kinetic energy cutoff of 700 eV was employed. The convergence threshold of 1×10^{-5} eV was set for the electronic energy and ionic relaxation proceeded until the atomic force was less than 0.05 eV·Å^{-1}. Grimme's approach (DFT + D3) has been incorporated to mimic the van der Waals interactions and dispersion-energy corrections. The Monkhorst–Pack grid was used to sample the first Brillouin zone. The $5 \times 5 \times 1$ k-point mesh was adopted for electronic structures analysis and geometric optimization [30]. A grid-based Bader charge analysing technique was used to determine the electron charge transfer [31].

In order to enhance comprehension and examination of the electronic structure, the projected density of states (PDOS) was computed [32]. Charge density difference ($\Delta\rho$) between the A and B fragments (ρ_A and ρ_B) and the combined A + B (ρ_{A+B}) was also computed by $\Delta\rho = \rho_{A+B} - \rho_A - \rho_B$, where ρ represents the total electron density.

Over NDG surface, the binding energy (E_b) of 3d-TM atoms was calculated as

$$E_b = E_{TM-N_4-G} - E_{NDG} - E_{TM} \quad (1)$$

where E_{TM-N_4-G} is the total energy of the whole system when the single metal atom is in the best adsorption position, E_{NDG} is the total energy of NDG substrate with one C vacancy, E_{TM} is the total energy of the single transition metal atom.

The free energy change (ΔG) for each elementary step of CORR was calculated based on the computational hydrogen electrode model [33] as

$$\Delta G = \Delta E + \Delta E_{ZPE} - T\Delta S + eU + k_B T \cdot pH \cdot \ln 1 \quad (2)$$

where ΔE is the total reaction energy, ΔE_{ZPE} is the correction of zero-point energy (ZPE), $T\Delta S$ is the entropy contribution and eU denotes the energy contributed by the applied electrode potential. k_B is kilobyte, T is the temperature. The pH in our work is set as zero, considering the strong acid environment. The free energy of $H^+ + e^-$ is equal to $1/2H_2$ under the standard conditions [34].

3 Results and discussion

3.1 Electronic structure of TM-N_4-G SACs and stability of bound single atoms

A system of nine 3d TM atoms are constructed on NDG [35]. The electronic structure of the catalysts and the binding strength of the TM heteroatoms to NDG were then calculated to assess the stability of these SACs.

The optimization results are shown in Fig. 1, where nine different metals are loaded on NDG, which exhibit relatively stable structure. Yang et al. investigated the reduction reaction using NDG with four nitrogen atoms loaded simultaneously with Ni, Co and Fe [36]. Similarly, Zhang et al. adopted the same NDG (with four nitrogen atoms) loaded with Fe atoms for the reduction reaction [37]. These examples demonstrate that the catalyst configuration used in this study is widely applied and offers significant advantages in terms of stability.

To further understand the structure of SACs, the d-orbital electronic structures of SACs are visualized in Figs. 2(a)–2(d) and Figs. S2(a)–S2(e) in the ESM. The density of states is projected onto the surface of the d-orbitals of the nine TMs embedded in double-vacancy, four NDG. When a small molecule interacts with a metal site, the empty d-orbital can accept electrons from the highest occupied molecular orbital (HOMO) and the occupied d-orbital can donate electrons to the lowest unoccupied molecular orbital (LUMO). It indicates that the d-band centers of all nine TMs are very close to the Fermi energy level. The adsorbate is more likely to provide charge to the metal sites, enhancing the interaction between the small molecule and the SACs [38]. The calculations show that d-

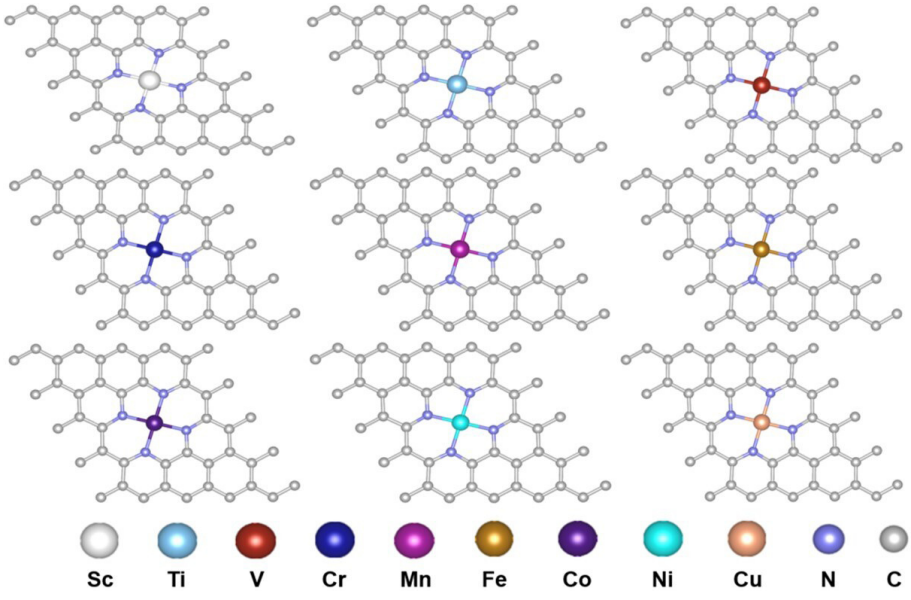

Figure 1 Top view of nine TM-N_4-G SACs.

band is sharper than that of the metal surface and is accompanied by a peak shift. This suggests the unique electronic structure of SACs can be leveraged for enhanced performance. Consequently, this distinctive electronic structure of SACs is expected to be applicable in a wider range of fields, potentially broadening the scope of use in various catalytic processes.

Building on this foundation, we calculated the binding energy (E_b) between TM and NDG substrate in Fig. 2(e). The strong binding stability suggests that all TM SACs can potentially be used as CORR catalysts. Sc-N_4-G SACs have the strongest binding energy (−8.5 eV) among them, while Cu-N_4-G SACs have a weak binding energy (−5.1 eV). Additionally, we performed Bader charge analysis of the catalysts (Table S1 in the ESM), which indicates electron transfer from the doped TM atom to the ligand site. The charge transfer between TM and NDG enhances the structural stability of SACs due to the ionic interactions between $TM^{\delta+}$ and $N^{\delta-}$ [39].

3.2 Adsorption energy of CO

Electrochemical CORR is a multiproton/electron transfer process involving various reaction intermediates and products. The first step in this process is the adsorption of CO at the TM site. TM atoms provide additional electrons to break the strong sp-hybridization, thus activating the CO molecule. Given the importance of CO adsorption for CORR, GGA calculations are used to identify the best adsorption sites on the catalyst and selected the top site. We calculated the adsorption energies for this site on each TM metal. While GGA functionals may overestimate CO binding on transition metals, we corrected the energy values and carefully studied the adsorption distance between CO and the catalyst. Therefore, this does not affect our conclusions about the strength of CO adsorption by the TM-N_4-G catalysts [40, 41]. As shown in Fig. 2(e), except for NDG supported by Ni and Cu atoms, which exhibit weak CO adsorption, the remaining TM-supported catalysts demonstrate very strong adsorption.

3.3 HER and CORR

Since the electrochemical reduction of CO takes place in an aqueous solution, where protons are supplied by the solution, the HER must be considered as it can compete with CORR and significantly affect the Faraday efficiency at low pH. To address this,

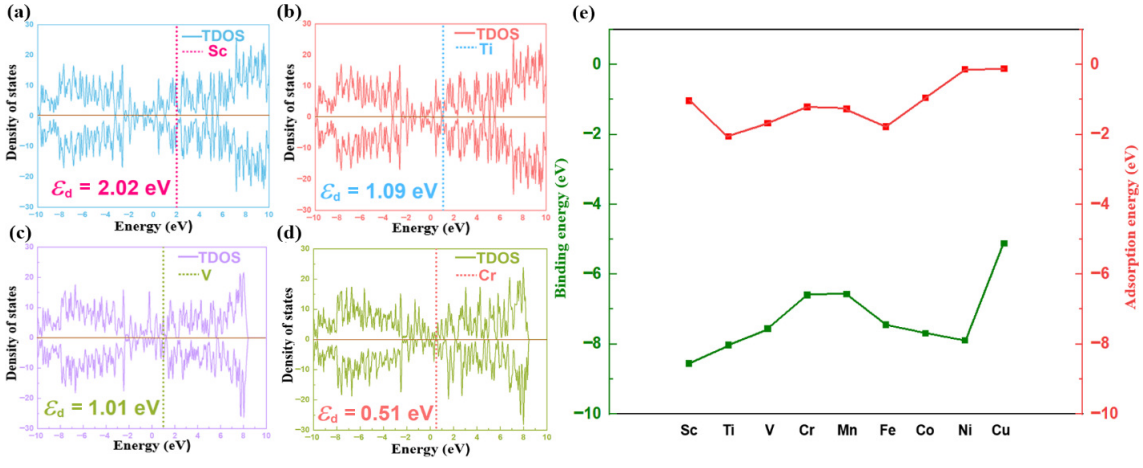

Figure 2 Density of states in the d orbitals (ε_d) of TM atoms (a) Sc-N_4-G SACs, (b) Ti-N_4-G SACs, (c) V-N_4-G SACs, (d) Cr-N_4-G SACs. (e) E_b and adsorption energy of CO on TM-N_4-G SACs.

we also examined the free energy change of HER, with the results shown in Fig. 3(a). The data indicate that all nine TM-based catalysts exhibit varying degrees of HER activity. Meanwhile, we compared the free energy change (ΔG) of the CO-to-*CO reaction with the ΔG of HER (Fig. 3(b)). The CO-to-*CO reaction is favored on all nine TM-N_4-G SACs. Additionally, the adsorption free energy (ΔG_{ads}) of *CO is more negative than that of *H and the ΔG for CO-to-*CO reduction is smaller than that for HER. Therefore, these SACs are more prone to CO adsorption and conversion compared to the occurrence of HER, indicating their higher selectivity for CORR over HER.

3.4 The choice of TM and the full path of CORR

As shown in Fig. 2(e), the adsorption energies for Cu-N_4-G and Ni-N_4-G are −0.13 and −0.1 eV. The GGA functionals might slightly overestimate CO adsorption strength. This indicates that Cu-N_4-G and Ni-N_4-G cannot effectively adsorb CO under normal conditions, so they were not included in the subsequent CORR pathway analyses. Meanwhile, the charge density differences for the remaining seven TM-N_4-G SACs with adsorbed CO are discussed (Figs. 4(a)–4(d) and Fig. S3 in the ESM). The results show a slight charge transfer between the metal sites and CO. However, practical experimental conditions such as temperature, pressure, solvent effects and dipole fields can enhance CO adsorption at the catalyst site.

On this basis, we conducted a detailed analytical study of the CORR pathway. The reduction of CO produces various products such as CH_2O, CH_3OH and CH_4. CH_2O can be generated from

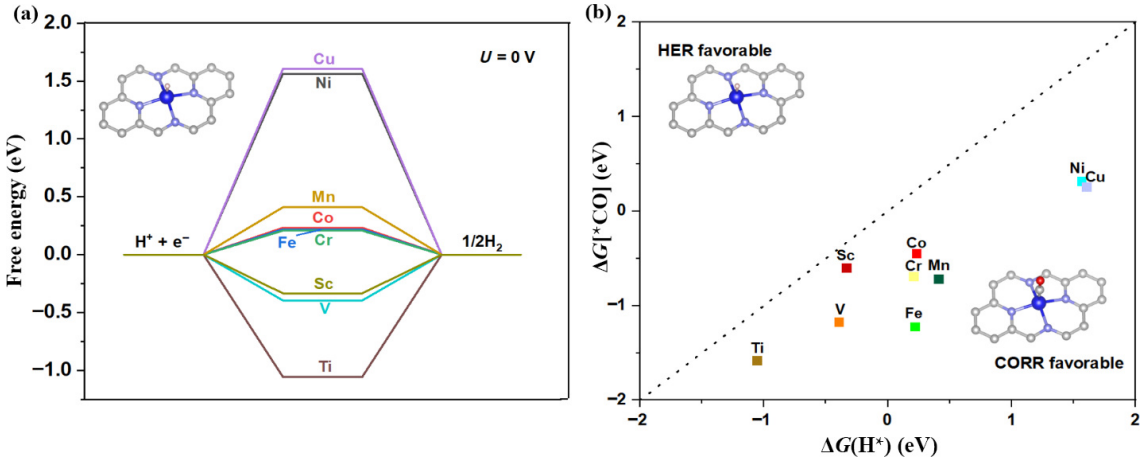

Figure 3 (a) Free energy of HER at the applied potential of voltage (U) = 0 V. (b) The Gibbs free energy of CO-to-*CO and HER on TM-N_4-G SACs.

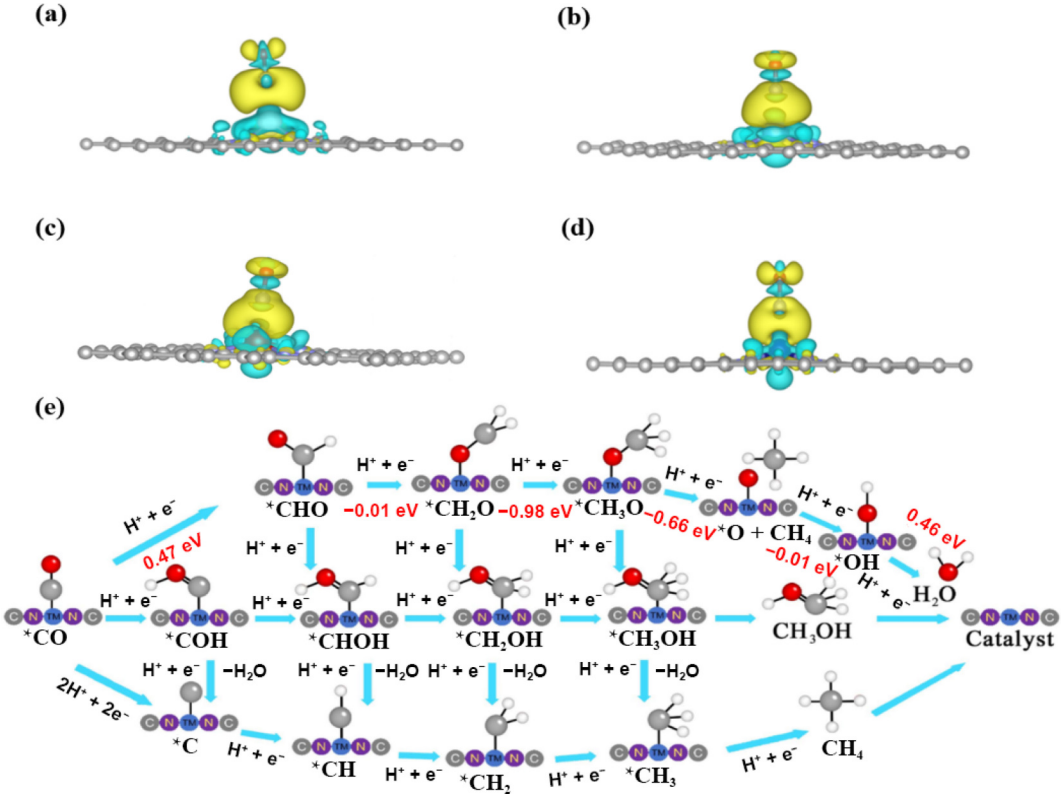

Figure 4 Isosurface of charge density difference ($\Delta\rho$) for CO adsorbed on (a) Sc-N_4-G SACs, (b) Ti-N_4-G SACs, (c) V-N_4-G SACs, (d) Cr-N_4-G SACs. Yellow: charge accumulation; cyan: charge depletion. (e) The reaction pathways for CO reduction to different C_1 products and the free energy contributions of intermediates.

*OCH_2 intermediates if the desorption energy is low, or alternatively from *CO via *CHO intermediates. The generation of CH_3OH involves intermediates such as *OCH_3 or *$OHCH_2$ and can proceed through multiple pathways. For the production of CH_4, two processes can occur: (i) Successive protonation reactions take place on C to produce CH_4 and *O. The *O is then converted to *OH by the continued addition of H^+ and is ultimately reduced to H_2O. (ii) Protonation reactions occur first on O to produce H_2O and *C, followed by deoxygenation of *C to produce CH_4. The process of hydrogenation reactions between C and O should also be considered. The detailed CORR mechanism, including the pathways and possible intermediates produced, is shown in Fig. 4(e).

The free energy paths of CORR on TM-N_4-G SACs have been calculated in Fig. 5. The results indicate that Cr-N_4-G SACs facilitate the gradual addition of H^+ to generate intermediate products such as *CHO, *CH_2O and *CH_3O, ultimately leading to the production of CH_4 and H_2O. This process effectively converts CO into the C_1 products CH_4 and H_2O.

During the conversion of CO by Cr-N_4-G SACs, the protonation of *CO to *CHO represents the largest free energy change step (ΔG = 0.47 eV), ultimately leading to the production of H_2O. Figure S4 in the ESM reveals that the limiting steps vary for different SACs. For Sc-N_4-G, Ti-N_4-G and V-N_4-G SACs, the limiting step is *OH to *H_2O. For Mn-N_4-G and Fe-N_4-G SACs, it shifts to *CO to *CHO. Finally, the limiting step is *CHO to *CH_2O for Co-N_4-G SACs. The goal is to identify the best catalysts with the fastest reaction rates and lowest energy requirements. In Fig. S5 in the ESM, Cr-N_4-G SACs have the lowest limiting step, while Ti-N_4-G SACs have the highest. Cr-N_4-G SACs has the best behavior among these catalysts for CORR, with optimal reaction speed and energy consumption. Under stable TM binding energy, favorable CO adsorption energy and the lowest limiting step in the reaction process, Cr is the optimal metal single-atom for CO reduction in this study.

4 Conclusion

In summary, we investigated the stability, adsorption, reaction pathways and screening of optimal TM SACs of transition metals (TM_1 = Sc, Ti, V, Cr, Mn, Fe, Co, Ni and Cu) single atoms loaded on NDG for CORR. The binding energies of single atoms from Sc to Cu on graphene indicate very stable bonding. The adsorption of HER and CO on TM SACs showed that CO adsorption is preferred over HER, thereby stabilizing CORR. At the same time, Cu-N_4-G and Ni-N_4-G were excluded due to their relatively weak CO adsorption. The CORR reduction steps were then investigated on the remaining TM SACs by calculating the free energies. Cr-N_4-G SACs had the lowest limiting step, demonstrating excellent performance with low energy consumption during CORR (limiting step is 0.47 eV). These results enhance the understanding of the electrochemical CORR reaction mechanism of SACs and provide valuable guidance for their design.

Electronic Supplementary Material: Supplementary material (the Bader charge of the TM catalysts and the charge density difference of the remaining TM catalysts as well as free energy step diagrams and rate limiting step comparison diagrams for catalysts) is available in the online version of this article at https://doi.org/10.26599/NR.2025.94907026.

Data availability

All data needed to support the conclusions in the paper are

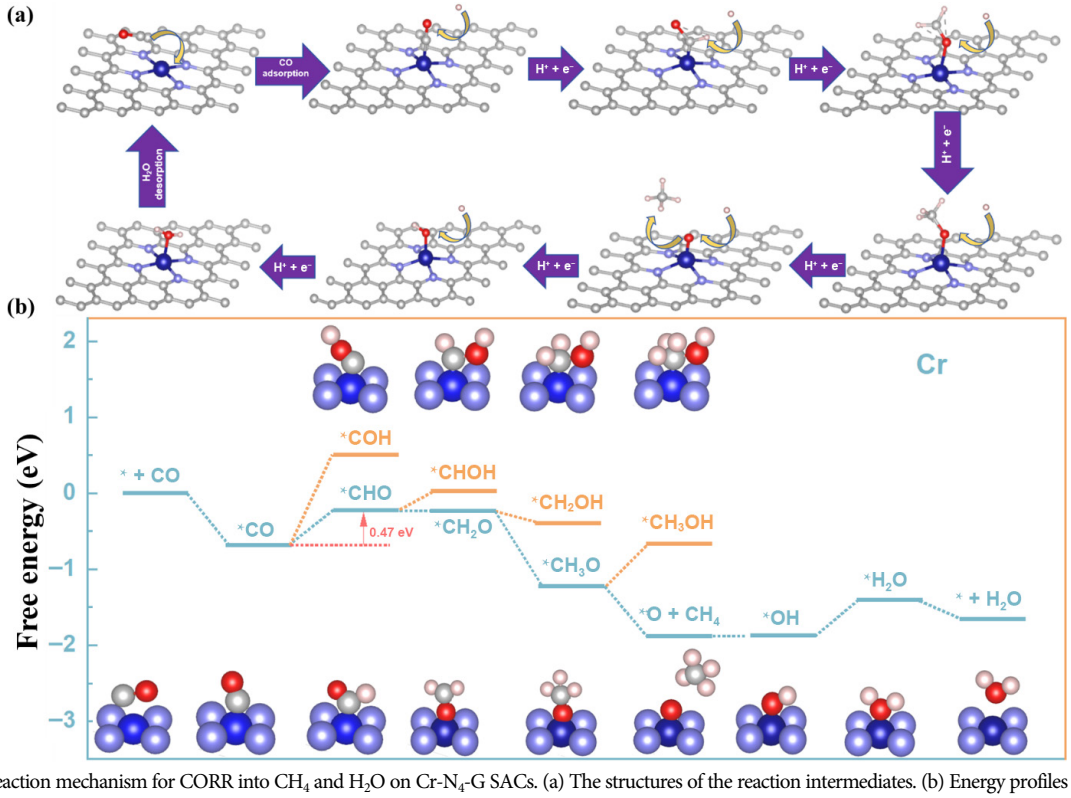

Figure 5 The reaction mechanism for CORR into CH_4 and H_2O on Cr-N_4-G SACs. (a) The structures of the reaction intermediates. (b) Energy profiles of different paths calculated by DFT method.

presented in the manuscript and the Electronic Supplementary Material. Additional data related to this paper may be requested from the corresponding author upon request.

Acknowledgements

This work was financially supported by the National Natural Science Foundation of China (No. 22473071) and Natural Science Basic Research Program of Shaanxi (Nos. 2021JCW-20 and 2022KJXX-18).

Declaration of competing interest

All the contributing authors report no conflict of interests in this work.

Author contribution statement

Q. Y. conceived and directed the research. Y. Z. G. performed the calculations. Y. Z. G. and S. H. T. co-wrote the paper. Q. Y., Y. Z. G., and S. H. T. designed the study, analyzed the data. All the authors discussed the results and commented on the manuscript. All the authors have approved the final manuscript.

Use of AI statement

None.

References

[1] Ji, Y. L.; Chen, Z.; Wei, R. L.; Yang, C.; Wang, Y. H.; Xu, J.; Zhang, H.; Guan, A. X.; Chen, J. T.; Sham, T. K. et al. Selective CO-to-acetate electroreduction via intermediate adsorption tuning on ordered Cu-Pd sites. *Nat. Catal.* **2022**, *5*, 251–258.

[2] Li, J.; Chang, X. X.; Zhang, H. C.; Malkani, A. S.; Cheng, M. J.; Xu, B. J.; Lu, Q. Electrokinetic and *in situ* spectroscopic investigations of CO electrochemical reduction on copper. *Nat. Commun.* **2021**, *12*, 3624.

[3] Xiang, S. Q.; Shi, J. L.; Gao, S. T.; Zhang, W.; Zhao, L. B. Thermodynamic and kinetic competition between C–H and O–H bond formation pathways during electrochemical reduction of CO on copper electrodes. *ACS Catal.* **2021**, *11*, 2422–2434.

[4] Tang, S. H.; Xu, L.; Dong, K. J.; Wang, Q. C.; Zeng, J.; Huang, X.; Li, H. T.; Xia, L. B.; Wang, L. L. Curvature effect on graphene-based Co/Ni single-atom catalysts. *Appl. Surf. Sci.* **2023**, *615*, 156357.

[5] Pan, C.; El-Khodary, S.; Wang, S.; Ling, Q. F.; Hu, X.; Xu, L. J.; Zhong, S. Research progress in graphene based single atom catalysts in recent years. *Fuel Process. Technol.* **2023**, *250*, 107879.

[6] Yu, Q. Theoretical studies of non-noble metal single-atom catalyst Ni_1/MoS_2: Electronic structure and electrocatalytic CO_2 reduction. *Sci. China Mater.* **2023**, *66*, 1079–1088.

[7] Ren, S.; Yu, Q.; Yu, X. H.; Rong, P.; Jiang, L. Y.; Jiang, J. C. Graphene-supported metal single-atom catalysts: A concise review. *Sci. China Mater.* **2020**, *63*, 903–920.

[8] Feng, S. X.; Yu, Q.; Ma, X. B.; Yu, X. H.; Yan, N. Hydroformylation over polyoxometalates supported single-atom Rh catalysts. *Natl. Sci. Open* **2023**, *2*, 20220064.

[9] Jiang, J. C.; Chen, J. C.; Zhao, M. D.; Yu, Q.; Wang, Y. G.; Li, J. Rational design of copper-based single-atom alloy catalysts for electrochemical CO_2 reduction. *Nano Res.* **2022**, *15*, 7116–7123.

[10] Yang, Q. Q.; Jiang, Y. F.; Zhuo, H. Y.; Mitchell, E. M.; Yu, Q. Recent progress of metal single-atom catalysts for energy applications. *Nano Energy* **2023**, *111*, 108404.

[11] Rong, P.; Jiang, Y. F.; Wang, Q.; Gu, M., Jiang, X. L.; Yu, Q. Photocatalytic degradation of methylene blue (MB) with Cu_1-ZnO single atom catalysts on graphene-coated flexible substrates. *J. Mater. Chem. A* **2022**, *10*, 6231–6241.

[12] Hai, X.; Zheng, Y.; Yu, Q.; Guo, N.; Xi, S. B.; Zhao, X. X.; Mitchell, S.; Luo, X. H.; Tulus, V.; Wang, M. et al. Geminal-atom catalysis for cross-coupling. *Nature* **2023**, *622*, 754–760.

[13] Jiang, L. Y.; Yang, Q. Q.; Xia, Z. M.; Yu, X. H.; Zhao, M. D.; Shi, Q. P.; Yu, Q. Recent progress of theoretical studies on electro- and photo-chemical conversion of CO_2 with single-atom catalysts. *RSC Adv.* **2023**, *13*, 5833–5850.

[14] Zhao, M. D.; Jiang, L. Y.; Yu, Q. Environmental applications of single-atom catalysts based on graphdiyne. *Catal. Sci. Technol.* **2023**, *13*, 5154–5174.

[15] Li, X. J.; Yu, X. H.; Yu, Q. Research progress on electrochemical CO_2 reduction for Cu-based single-atom catalysts. *Sci. China Mater.* **2023**, *66*, 3765–3781.

[16] Ma, T.; Fan, Q.; Li, X.; Qiu, J. S.; Wu, T. B.; Sun, Z. Y. Graphene-based materials for electrochemical CO_2 reduction. *J. CO_2 Util.* **2019**, *30*, 168–182.

[17] Ghosh, S.; Calizo, I.; Teweldebrhan, D.; Pokatilov, E. P.; Nika, D. L.; Balandin, A. A.; Bao, W.; Miao, F.; Lau, C. N. Extremely high thermal conductivity of graphene: Prospects for thermal management applications in nanoelectronic circuits. *Appl. Phys. Lett.* **2008**, *92*, 151911.

[18] Yu, Q.; Jiang, J. C.; Jiang, L. Y.; Yang, Q. Q.; Yan, N. Advances in green synthesis and applications of graphene. *Nano Res.* **2021**, *14*, 3724–3743.

[19] Zhuo, H. Y.; Zhang, X.; Liang, J. X.; Yu, Q.; Xiao, H.; Li, J. Theoretical understandings of graphene-based metal single-atom catalysts: Stability and catalytic performance. *Chem. Rev.* **2020**, *120*, 12315–12341.

[20] Chen, Z. P.; Mou, K. W.; Yao, S. Y.; Liu, L. C. Zinc-coordinated nitrogen-codoped graphene as an efficient catalyst for selective electrochemical reduction of CO_2 to CO. *ChemSusChem* **2018**, *11*, 2944–2952.

[21] Liu, J. C.; Ma, X. L.; Li, Y.; Wang, Y. G.; Xiao, H.; Li, J. Heterogeneous Fe_3 single-cluster catalyst for ammonia synthesis via an associative mechanism. *Nat. Commun.* **2018**, *9*, 1610.

[22] Wang, J.; You, R.; Zhao, C.; Zhang, W.; Liu, W.; Fu, X. P.; Li, Y. Y.; Zhou, F. Y.; Zheng, X. S.; Xu, Q. et al. N-coordinated dual-metal single-site catalyst for low-temperature CO oxidation. *ACS Catal.* **2020**, *10*, 2754–2761.

[23] Wu, T. J.; Lin, J.; Cheng, Y.; Tian, J.; Wang, S. W.; Xie, S. H.; Pei, Y.; Yan, S. R.; Qiao, M. H.; Xu, H. L. et al. Porous graphene-confined Fe-K as highly efficient catalyst for CO_2 direct hydrogenation to light olefins. *ACS Appl. Mater. Interfaces* **2018**, *10*, 23439–23443.

[24] Tao, H. C.; Sun, X. F.; Back, S.; Han, Z. S.; Zhu, Q. G.; Robertson, A. W.; Ma, T.; Fan, Q.; Han, B. X.; Jung, Y. et al. Doping palladium with tellurium for the highly selective electrocatalytic reduction of aqueous CO_2 to CO. *Chem. Sci.* **2018**, *9*, 483–487.

[25] Wang, H.; Li, Y. Z.; Wang, M. Y.; Chen, S.; Yao, M.; Chen, J. L.; Liao, X. L.; Zhang, Y. W.; Lu, X.; Matios, E. et al. Precursor-mediated *in situ* growth of hierarchical N-doped graphene nanofibers confining nickel single atoms for CO_2 electroreduction. *Proc. Natl. Acad. Sci. USA* **2023**, *120*, e2219043120.

[26] Sun, Q.; Jia, C.; Zhao, Y.; Zhao, C. Single atom-based catalysts for electrochemical CO_2 reduction. *Chin. J. Catal.* **2022**, *43*, 1547–1597.

[27] Blöchl, P. E. Projector augmented-wave method. *Phys. Rev. B* **1994**, *50*, 17953–17979.

[28] Kresse, G.; Joubert, D. From ultrasoft pseudopotentials to the projector augmented-wave method. *Phys. Rev. B* **1999**, *59*, 1758–1775.

[29] Perdew, J. P.; Burke, K.; Ernzerhof, M. Generalized gradient approximation made simple. *Phys. Rev. Lett.* **1996**, *77*, 3865–3868.

[30] Monkhorst, H. J.; Pack, J. D. Special points for Brillouin-zone integrations. *Phys. Rev. B* **1976**, *13*, 5188–5192.

[31] Bader, R. F. W. A quantum theory of molecular structure and its applications. *Chem. Rev.* **1991**, *91*, 893–928.

[32] Maintz, S.; Deringer, V. L.; Tchougréeff, A. L.; Dronskowski, R. Analytic projection from plane-wave and PAW wavefunctions and application to chemical-bonding analysis in solids. *J. Comput. Chem.* **2013**, *34*, 2557–2567.

[33] Nørskov, J. K.; Rossmeisl, J.; Logadottir, A.; Lindqvist, L.; Kitchin, J. R.; Bligaard, T.; Jónsson, H. Origin of the overpotential for oxygen reduction at a fuel-cell cathode. *J. Phys. Chem. B* **2004**, *108*, 17886–17892.

[34] Peterson, A. A.; Nørskov, J. K. Activity descriptors for CO_2 electroreduction to methane on transition-metal catalysts. *J. Phys. Chem. Lett.* **2012**, *3*, 251–258.

[35] Bi, W. T.; Li, X. G.; You, R.; Chen, M. L.; Yuan, R. L.; Huang, W. X.; Wu, X. J.; Chu, W. S.; Wu, C. Z.; Xie, Y. Surface immobilization of transition metal ions on nitrogen-doped graphene realizing high-efficient and selective CO_2 reduction. *Adv. Mater.* **2018**, *30*, 1706617.

[36] Yang, Y.; Li, J. Y.; Zhang, C. Y.; Yang, Z. Q.; Sun, P. L.; Liu, S. X.; Cao, Q. E. Theoretical insights into nitrogen-doped graphene-supported Fe, Co, and Ni as single-atom catalysts for CO_2 reduction reaction. *J. Phys. Chem. C* **2022**, *126*, 4338–4346.

[37] Zhang, C. H.; Yang, S. Z.; Wu, J. J.; Liu, M. J.; Yazdi, S.; Ren, M. Q.; Sha, J. W.; Zhong, J.;Nie, K. Q.; Jalilov, A. S. et al. Electrochemical CO_2 reduction with atomic iron-dispersed on nitrogen-doped graphene. *Adv. Energy Mater.* **2018**, *8*, 1703487.

[38] Mun, Y.; Lee, S.; Kim, K.; Kim, S.; Lee, S.; Han, J. W.; Lee, J. Versatile strategy for tuning ORR activity of a single Fe-N_4 site by controlling electron-withdrawing/donating properties of a carbon plane. *J. Am. Chem. Soc.* **2019**, *141*, 6254–6262.

[39] Lin, S.; Ye, X. X.; Johnson, R. S.; Guo, H. First-principles investigations of metal (Cu, Ag, Au, Pt, Rh, Pd, Fe, Co, and Ir) doped hexagonal boron nitride nanosheets: Stability and catalysis of CO oxidation. *J. Phys. Chem. C* **2013**, *117*, 17319–17326.

[40] Irmer, S.; Kochan, D.; Lee, J.; Fabian, J. Resonant scattering due to adatoms in graphene: Top, bridge, and hollow positions. *Phys. Rev. B* **2018**, *97*, 075417.

[41] Feibelman, P. J.; Hammer, B.; Nørskov, J. K.; Wagner, F.; Scheffler, M.; Stumpf, R.; Watwe, R.; Dumesic, J. The CO/Pt (111) puzzle. *J. Phys. Chem. B* **2001**, *105*, 4018–4025.